ORIGINAL PAPER

ANALYSIS OF SINTERED Zr_XEr_{1-X} OBTAINED THROUGH POWDER METALLURGY

NICOLAE TIBERIU CIOBANU[1,2], DENIS AURELIAN NEGREA[3], MARIANA POSTELNICU[1], NINA GABRIELA TUDORACHE[1], NICOLAE VALENTIN OLARU[1], AUREL DAVID[1]

Manuscript received: 17.07.2024;Accepted paper: 04.12.2024;
Published online: 30.12.2024.

Abstract. *This paper aims to analyze Zr-Er sintered compounds obtained through powder metallurgy, with different concentrations, able to store H_2. To obtain Zr-Er sintered compacts, in the first phase, zirconium and erbium were hydrides separately, at 750°C in a hydrogen atmosphere, for two hours each, to obtain zirconium and erbium hydrides. Using XRD analysis, both zirconium and erbium formed ErH_3 and ZrH_2. After the mechanical processing, morphological analysis performed by scanning electron microscopy and energy dispersive X-ray spectroscopy (SEM-EDS) revealed microparticles with sizes ranging from 8.08 µm to 27.16 µm for ZrH_2, 3.72 µm to 17.86 µm for ErH_3. The mixtures of hydride powders were pressed in a cylindrical mold, and two Zr_xEr_{1-x}(x=0.25;0.75) pressed compacts were obtained. These samples were subjected to a heat treatment, in a helium atmosphere, that included a dehydrogenation treatment, followed by a sintering treatment, at 1200°C, for two hours. The compounds obtained were geometrically characterized, their experimentally determined density being more than 90% of their calculated density. SEM analysis of the sintered compounds revealed a densification of zirconium and erbium particles, and also, the higher the zirconium content, the more pores the sintered sample has. SEM-EDS microstructural analysis shows a uniform distribution of the component elements, and an increased tendency of erbium to oxidize.*

Keywords: *hydrides; sintering; powder metallurgy; zirconium; erbium.*

1. INTRODUCTION

Globally, this chemical element is considered the second energy source, as an energy carrier. Energy is delivered, stored, and transported in an easily usable form by the energy carrier. Additionally, hydrogen is a potential energy source for the future due to its ease of storage in a variety of forms. It is effective; it typically produces very little pollution, and it may be applied to heat and electricity production, as well as to transportation [1].

To use the hydrogen as an energy source, it has to be stored. This gas can be stored using different methods, such as gas storage in pressure vessels, liquid storage, and solid storage [1]. The solid storage can be performed using metals or metal alloys. In this sense, research and development works of new materials with a large storage capacity are necessary.

[1] Institute for Nuclear Research, Nuclear Materials and Corrosion, 115400 Pitesti, Romania.
E-mail: tiberiu.ciobanu@nuclear.ro.
[2] National University of Science and Technology POLITEHNICA Bucharest, Pitesti University Centre, Doctoral School Materials Science and Engineering, 110040 Pitesti, Romania.
[3] National University of Science and Technology POLITEHNICA Bucharest, Pitesti University Centre, Regional center of research & development for materials, processes and innovative products dedicated to the automotive industry (CRC&D-AUTO), 110440 Pitesti, Romania. E-mail: aurelian.negrea@upb.ro.

https://doi.org/10.46939/J.Sci.Arts-24.4-b06

In this work, an experimental study was chosen on obtaining sintered Zr-Er composites, with different compositions, using powder metallurgy. These materials, zirconium, and erbium, were chosen because they both could store hydrogen [2,3]. To obtain those compounds, the powder metallurgy method was chosen instead of the process of obtaining alloys by melting, because it offers several advantages, such as *(i)* quality, the compounds obtained through powder metallurgy are protected from oxidation that may occur during the manufacturing process [4]; *(ii)* material implications, powder metallurgy allows far greater flexibility in material usage and alloy choice [4,5]; *(iii)* costs, compared to melting, using the production of alloys through powder metallurgy, the mechanical processing of the obtained compacts is not necessary, and the energy consumption is lower, melting metal is energy-intensive, and more so for materials with a higher melting point [5].

2. MATERIALS AND METHODS

2.1. MATERIALS

To obtain Zr_xEr_{1-x} compounds (where x=0.25 and 0.75), were prepared: zirconium sponge, with a purity of over 99%, from the supplier Wah Chang, Albany, U.S.A., metallic erbium, with a purity of over 99.9%, from Hefa Rare Earth Canada and hydrogen 6.0, with a purity of over 99.999%, from the Linde Company, Romania. Fig. 1 represents the flow sheet required to obtain Zr-Er compounds.

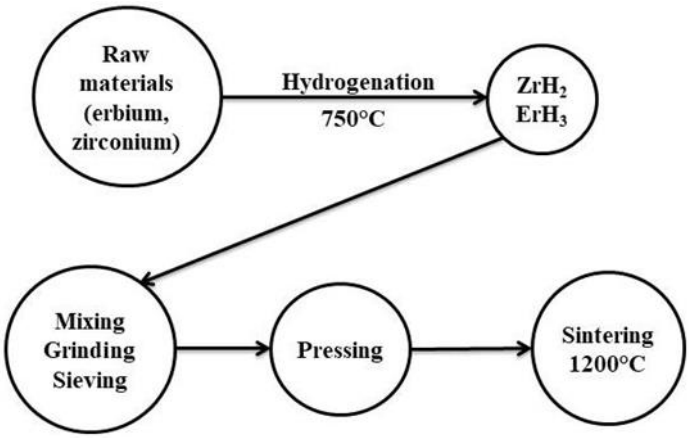

Figure 1. The flow sheet for obtaining Zr-Er compacts, using powder metallurgy

2.2. PREPARATION OF HYDRIDES

The hydrogenation of the raw materials was chosen to embrittle the component materials, thus facilitating their processing.

According to the phase diagram between zirconium and hydrogen (Fig. 2), it interacts with hydrogen at a temperature of 750^{o}C, forming ZrH_2.

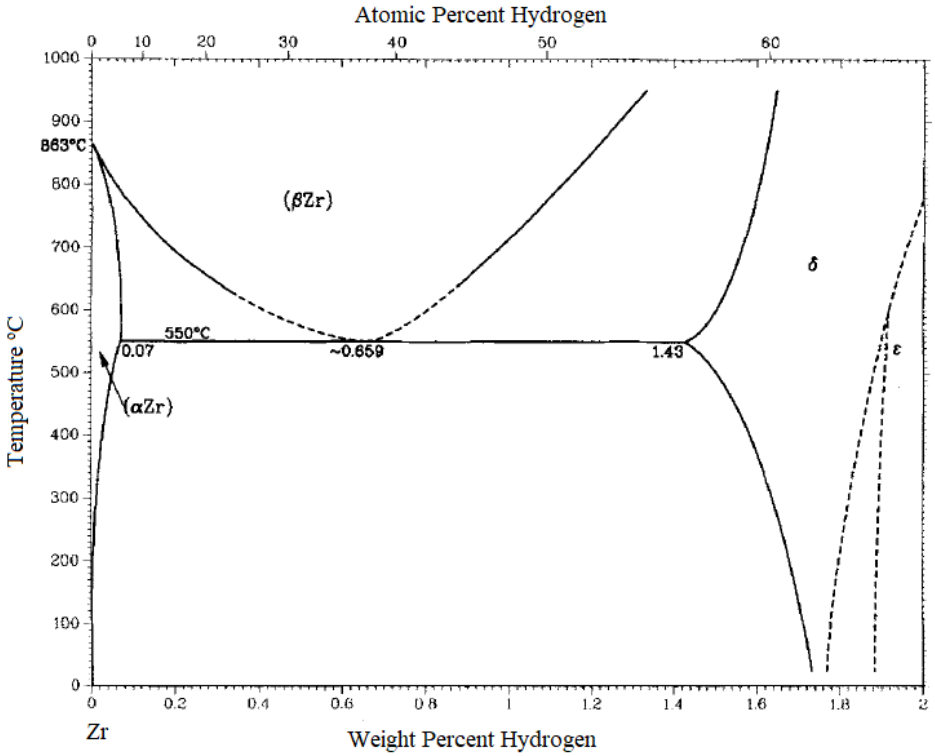

Figure 2. Phase diagram Zr-H, adapted from [2]

The hydrogenation treatment was carried out in a thermal furnace at the previously mentioned temperature for two hours. Initially, the furnace chamber was emptied to eliminate the gas residues, after which the hydrogen supply was started. The hydrogenation treatment was carried out in a dynamic gas atmosphere. After the hydrogenation treatment, a quantity of zirconium hydride was obtained (Fig. 3). From Fig. 3 it can be seen that zirconium did not change its geometric properties, following the interaction with hydrogen.

Figure 3. Zirconium hydride

Erbium hydride was carried out under the same conditions as in the case of zirconium. The hydrogenation of erbium was performed at a temperature of 750^{o}C for 2 hours [3]. Following this treatment, a quantity of erbium hydride was obtained (Fig. 4). It is observed that the interaction between erbium and hydrogen differs from that of zirconium, because erbium, after hydrogenation, completely loses its geometric properties, erbium hydride being in the form of granules with a maximum diameter of 5 mm. It can be also observed that erbium hydride has a different colour than metallic erbium (light grey).

Figure 4. Erbium hydride

2.3. OBTAINING THE COMPACTS

After hydrogenation, the powders were weighed and dosed to obtain 2 batches of the following amounts: 75%ZrH_2-25%ErH_3, 25%ZrH_2-75%ErH_3. The hydrides were hand-mixed and ground using a pestle mortar. Afterward, the ground powders were sieved through special sieves, made of stainless steel, with a grain size of up to 32 μm. Through this step, controlled granulation of the aforementioned powders is ensured. The powders that did not reach the desired granulation (up to 32 μm), were ground again, the entire process was repeated until all quantities of powders reached the previously mentioned granulation. All these operations were carried out in a box sealed with gloves.

The batches of powders obtained were manually loaded into a cylindrical stainless steel mold, which has a diameter of 15.5 mm. The pressing of the powders was done manually, using a one-sided press. The first time it was tried to press the powders at a pressure of $8*10^6$ Pa, but it was not possible to obtain pressed compacts. After that, another attempt was made to press the powders, at a pressure of approximately $11.5 \cdot 10^6$ Pa, for 15 seconds each, after which it was possible to obtain the desired pressed compacts. Following the mixing, grinding, sieving, and pressing processes, two samples of $_xZrH_2$-$_{(1-x)}ErH_3$ (x=0.25;0.75) were obtained. Table 1 presents the characteristics of the pressed samples.

Table 1. Geometric properties of pressed samples

Sample number	Content	Geometric density (g/cm^3)
Sample 1	75%ZrH_2-25%ErH_3	4.509
Sample 2	25%ZrH_2-75%ErH_3	5.128

2.4. SINTERING PROCEDURE

In the final stage, the pressed samples were sintered in a thermal furnace, in the atmosphere dynamic He 6.0, at a pressure of 10^5 Pa, the working temperature being 2/3 of the melting temperature of the material with the higher melting point ($T_{melting}$Er=1529^{o}C, $T_{melting}$Zr=1855^{o}C) [6]. Also, the selection of the working temperature is followed by complete dehydrogenation of the samples. The sintering of the pressed compacts was carried out as follows:

I. 25 – 400^{o}C (heating rate 10^{o}C/minute);
II. 400 – 650^{o}C (heating rate 15^{o}C/minute);

III. 650 – 775°C (heating rate 10°C/minute);
IV. 775 – 850°C (heating rate 1°C/minute, dehydrogenation level);
V. 850 – 850°C (20 minutes, for dehydrogenation);
VI. 850 – 1200°C (heating speed 10°C/minute);
VII. 1200 – 1200°C (120 minutes, samples sintering).

The cooling of the furnace enclosure was carried out freely, its duration being approximately 120 minutes.

2.5. ANALYTICAL TECHNIQUES

After the hydrogenation treatments of the Zr and Er raw materials, the obtained hydrides were analyzed in terms of microstructure through X-ray diffraction using the 'PANALYTICAL X'PERT PRO MPD' computerized diffractometer (Malvern Panalytical Ltd, Malvern United Kingdom), with Bragg-Brentano geometry and an X-ray ceramic source, with the Cu Kα anode (λ=1.540 Å). The detector used is an X'Celerator which is an ultra-fast X-ray detector based on Real Time Multiple Strip (RTMS) technology. The diffractograms were taken in the 2θ range from 20° to 150°, using a scanning rate of 1°/min, at room temperature.

The morphology and particle sizes of the erbium and zirconium hydrides, and also for the sintered compounds of $Zr_xEr_{(1-x)}$(x=0.25;0.75), were analyzed using Tescan `VEGA II LMU` scanning electron microscope (TESCAN GROUP, Brno – Kohoutovice, Czech Republic), in a vacuum, at a pressure of $5.0 \cdot 10^{-2}$ Pa.

The sintered compounds of $Zr_xEr_{(1-x)}$(x=0.25;0.75) were geometrically characterized by measuring their diameter, height, and weight. The densities of the samples were determined experimentally by immersion in demineralized water, at atmospheric pressure and room temperature, using an analytical balance of the RADWAG XA 160/X type (RADWAG Headquarters, Poland).

The microstructural analysis of the Zr_x-$Er_{(1-x)}$(x=0.75;0.25) sintered samples was carried out using a HITACHI SU5000 scanning electron microscope equipped with an energy dispersive X-ray spectroscopy (EDS) module (Hitachi, Tokyo, Japan) for chemical element analysis.

3. RESULTS AND DISCUSSION

3.1. STRUCTURAL AND MORPHOLOGICAL CHARACTERIZATION OF PRECURSOR POWDERS

The first step of characterization of the obtained erbium hydride and zirconium hydride powders was analyzed by X-ray diffraction, to determine the phases formed after the hydrogenation treatments.

Fig. 5 shows the XRD spectrum of the erbium hydride powder. The analysis shows that the erbium was almost completely hydrated, forming ErH_3, with a hexagonal crystal structure, space group $P63/mm^3$, and lattice parameters a=3.621 Å, c=6.525 Å, and the presence of erbium oxide, in the form of $ErO_{1.5}$, and erbium hydroxide, in the form of ErOH, is also noted in small quantities, both having a cubic crystal structure, according to ICDD

PDF4+. The morphological properties of the ErH_3 obtained are in good agreement with the existing results in the literature [7,8].

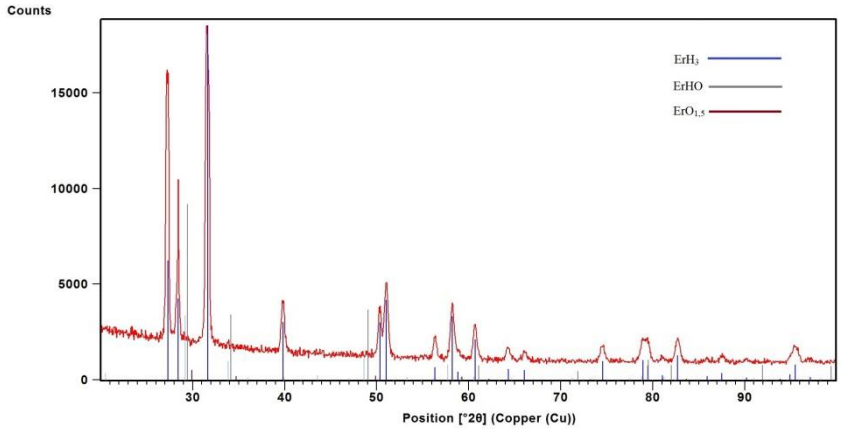

Figure 5. XRD patterns of erbium hydrides powder

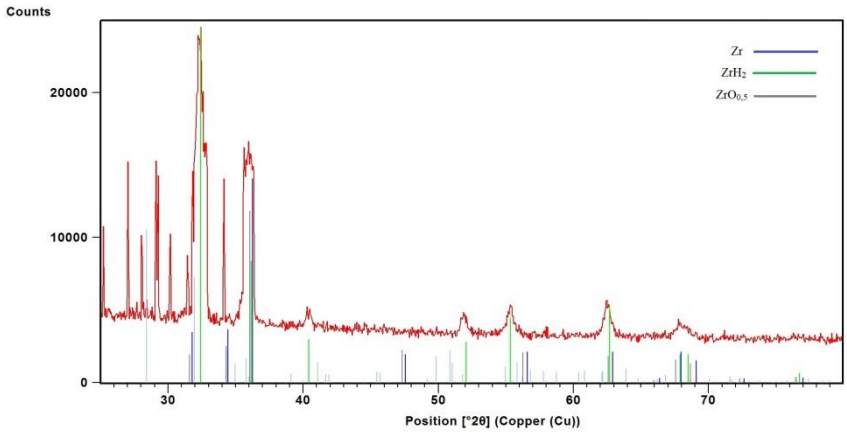

Figure 6. XRD patterns of zirconium hydride powder.

Following the XRD spectrum of zirconium hydride powders (Fig. 6), it is found that the zirconium was partially hydrated, forming ZrH_2, with a tetragonal crystal system, space group I4/mmm and lattice parameters a=3.51 Å, c=4.46Å, and the presence of zirconium oxide, in the form of $ZrO_{0.5}$, in small quantities, with a hexagonal crystalline structure, according to ICDD PDF4+. The oxide found in the analysis powders is caused by the mechanical processing that was carried out in the free atmosphere. Properties determined through X-ray diffraction of ZrH_2 are in good agreement with experimental results existing in the literature [8-11].

After XRD, the mixture of hydride powders was characterized by scanning electron microscopy (SEM). The samples were analyzed using the Tescan `VEGA II LMU` microscope, in a vacuum, at a pressure of $5*10^{-2}$ Pa. In Fig. 7, the SEM analysis of the powder with a composition of 75%ZrH_2-25%ErH_3, and Fig. 8 shows the SEM analysis of the powder with a composition of 25%ZrH_2-75%ErH_3.

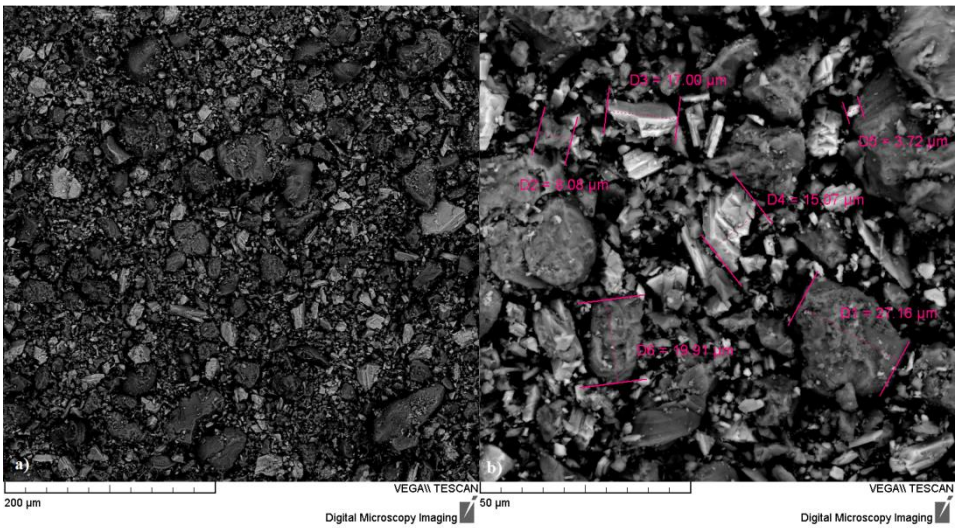

Figure 7. a) SEM analyse of $75ZrH_2$-$25ErH_3$, resolution x500, using BSE detector; b) SEM analyse of $75ZrH_2$-$25ErH_3$, resolution x2000, using BSE detector.

Fig. 7.a) shows the increased density of ZrH_2 particles (dark grey particles) and the low presence of ErH_3 particles (light grey). The color difference between the two elements is given by the atomic number, the element in the analysis with a higher atomic number has a lighter color than the other elements. In Fig. 7.b), the size of the hydride particles was determined, using the processing program provided with the device. To measure the size of a hydride particle, the edges of the selected particles must be delimited, after which the analysis program determines, through calculations, what is the distance between the boundaries of the selected area. The size of zirconium hydride particles is between 8.08 µm and 27.16 µm, and in the case of erbium hydride, the size of the particles is between 3.72 µm and 17 µm.

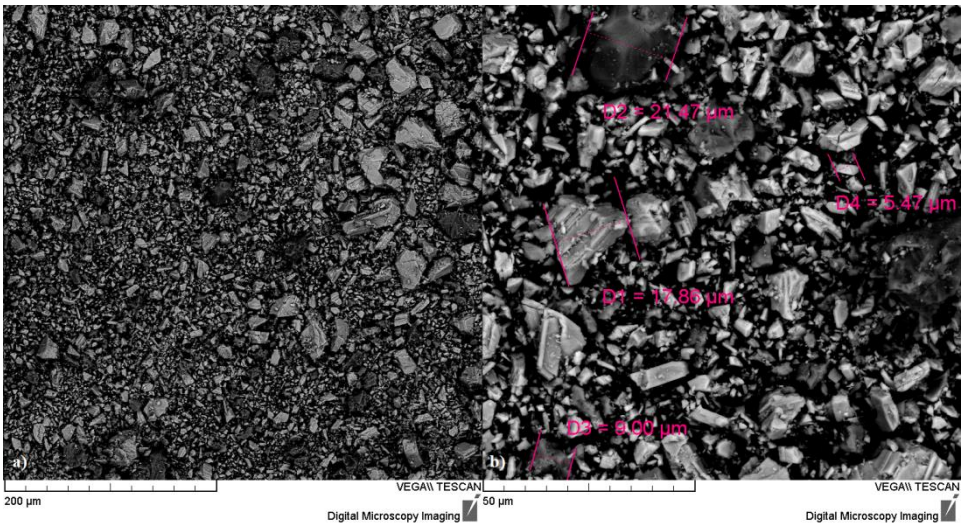

Figure 8. a) SEM image of $25ZrH_2$-$75ErH_3$, resolution x500, using BSE detector; b) SEM image of $25ZrH_2$-$75ErH_3$, resolution x2000, using BSE detector.

Fig. 8.a) shows an increased occurrence of ErH_3 particles (light grey particles) and the low presence of ZrH_2 particles (dark grey). Fig. 8.b), the grain size of the hydride mixture was determined, using the processing program provided with the device. The size of zirconium hydride particles is between 9.0 µm and 21.47 µm, and in the case of erbium hydride, the size of the particles is between 5.47 µm and 17.86 µm.

3.2. STRUCTURAL AND MORPHOLOGICAL ANALYSES OF SINTERED SAMPLES

As stated previously, two samples of Zr_x-$Er_{(1-x)}$(x=0.25;0.75) were obtained following the sintering process (Table 2).

Table 2. Geometric properties of $Zr_xEr_{(1-x)}$ sintered compounds

Sample number	Content	Form	Height (mm)	Diameter (mm)
Sample 1	75%Zr-25%Er	cylindrical	10.75	13.75
Sample 2	25%Zr-75%Er	cylindrical	15.46	13.45

The first step in analyzing the samples was to determine their density. Determination of the density of the sintered compacts was carried out by immersion in demineralized water, using an analytical balance of the RADWAG XA 160/X type (Table 3). To be able to make a comparison about the quality of the sintered compounds, the theoretical densities of the compacts were previously determined using the following Equation (1):

$$\rho_{theoretical}(g/cm^3) = \frac{1}{(\frac{WZr}{\rho Zr}+\frac{WEr}{\rho Er})} \quad (1)$$

where W_{Zr} and W_{Er} are the weight fractions of zirconium and erbium, while ρ_{Zr} and ρ_{Er} are the densities of zirconium and erbium. It can be observed that the second sample, which contains a larger amount of erbium, has a higher density than the sample with a high zirconium content, this is due to the high density of erbium (ρ_{Er}=9.07 g/cm^3) [6].

Table 3. Experimental and theoretical densities of the Zr-Er sintered compounds

Sample number	Content	Weight [g]	Experimental density [g/cm^3]	Theoretical density [g/cm^3]
Sample 1	$Zr_{0.75}Er_{0.25}$	9.48	6.71	7.16
Sample 2	$Zr_{0.25}Er_{0.75}$	16.54	7.7	8.52

To determine the morphology of particles, the samples were analyzed by scanning electron microscopy, and the results were presented in Figs. 9 and 10.

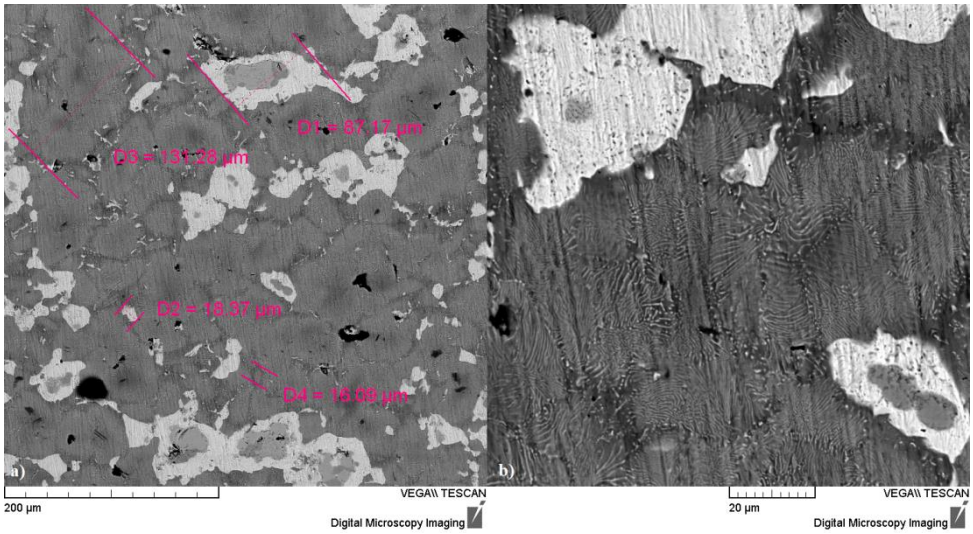

Figure 9. a) SEM image of $Zr_{0.75}Er_{0.25}$ sintered compound, resolution x500, using BSE detector; b) SEM image of $Zr_{0.75}Er_{0.25}$ sintered compound; resolution x2000, using BSE detector.

Fig. 9.a) shows the zirconium particles, with dark grey, and the size of the zirconium particles (these particles have a maximum particle size of 131.28 μm). Due to the larger content of Zr, in this sample, an increased porosity on the analyzed surface (black areas) can be seen. The large size of the particles is due to the fusion effect that occurs during sintering. In Fig. 9.b) the presence of erbium in zirconium can be observed, this is a result of the solubility of erbium in zirconium, during the sintering level ($T_{sintering}$=1200^oC).

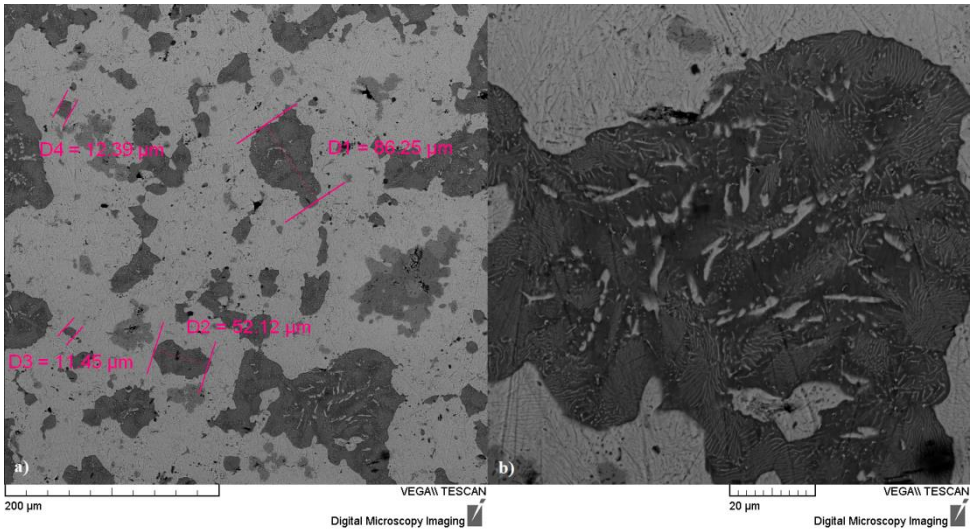

Figure 10. a) SEM image of $Zr_{0.25}Er_{0.75}$ sintered compund, resolution x500, using BSE detector; b) SEM image of $Zr_{0.25}Er_{0.75}$ sintered compound, resolution x2000, using BSE detector.

In Fig. 10.a) an abundance of erbium can be observed (light gray area), the space between the erbium particles being almost non-existent, which is achieved by the fusion that occurred during sintering. Also, the porosity in this sample (black areas) is almost nonexistent, due to the low content of zirconium. The sizes of zirconium particles (dark grey) can reach up to 86.25 μm. These dimensions were determined using the electron microscope analysis program. The first step to measure the size of a specific particle is to delimit the edges of the selected particle, after which the analysis program determines, through calculations, what is the distance between the boundaries of the respective area. Fig. 11 shows the results of SEM-EDS microstructural analysis of the $Zr_{0.75}Er_{0.25}$ sample.

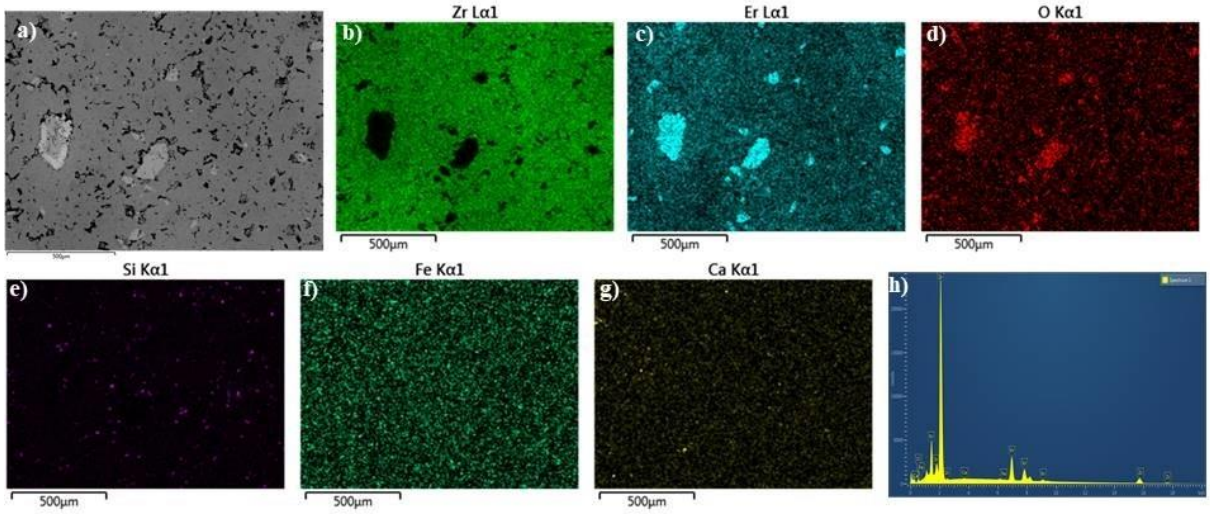

Figure 11. a) SEM analysis of $Zr_{0.75}Er_{0.25}$ sintered compound, magnification x90, using BSE detector, (b)-(g) Zr, Er, O, Si, Fe, and Ca elemental distribution; h) EDS scanning results of sample content.

Fig. 11.a) shows the micrograph of the sample containing $Zr_{0.75}Er_{0.25}$, at a magnification of x90, using a backscattered electron (BSE) detector, in which it can be observed the predominant presence of Zr (dark grey), much less presence of erbium (light grey) and the existence of pores on the entire analyzed surface (black areas). Figs. 11. b) - 11. g) show the distribution of the elements found in the composition of the analyzed sample. From these figures, it can be observed the presence of erbium in the zirconium matrix, due to the solubility phenomenon that occurred during the sintering treatment, the presence of oxygen in the sample, especially in the areas with an increased concentration of erbium, and the low presence of the other elements (Si, Fe, and Ca), this is due to impurities in the raw materials used to obtain these sintered compounds. Fig. 11.h) shows the results obtained by EDS area scanning of the component elements from the $Zr_{0.75}Er_{0.25}$ sample.

Table 4 presents the results of the quantitative analysis of the $Zr_{0.75}Er_{0.25}$ sample, obtained from the EDS analyses.

Table 4. Results of the quantitative analysis of sample $Zr_{0.75}Er_{0.25}$

Chemical elements	Composition measured by weighing [wt.%]	Composition measured by EDS [wt.%]	Sigma [wt.%]
Zr	75	64.25	0.20
Er	25	29.26	0.18
O		5.49	0.15
Si		0.72	0.04
Fe		0.17	0.05
Ca		0.11	0.03

Fig. 12 shows the results of SEM-EDS microstructural analysis on the $Zr_{0.25}Er_{0.75}$ sample.

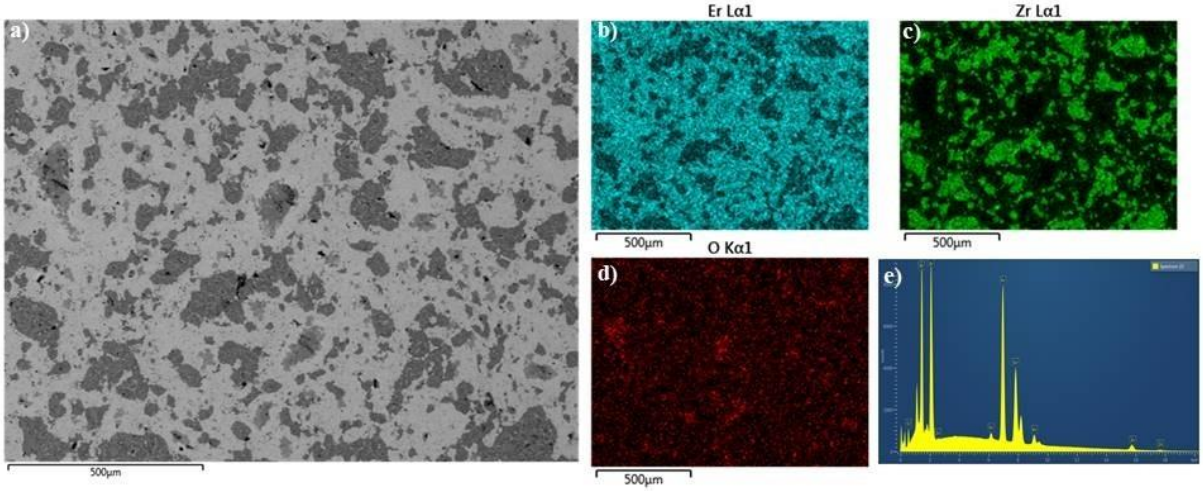

Figure 12. a) SEM analysis of $Zr_{0.25}Er_{0.75}$ sintered compound, resolution x90, using BSE detector; (b)-(d) Zr, Er and O elemental distribution; e) EDS scanning results of sample content.

Fig. 12.a) shows the micrograph of the $Zr_{0.25}Er_{0.75}$ sample, at a magnification of x90, using a BSE type detector, in which found the predominant presence of Er, the erbium content being associated with the light grey areas, the much lower presence of zirconium, this element is associated with the dark grey areas and the much lower existence of pores, compared to the $Zr_{0.75}Er_{0.25}$ sample, over the entire analyzed surface (black areas). Figs. 12. b)-12.d) show the distribution of the elements found in the composition of the analyzed sample. According to the analyses, it is possible to observe areas where both erbium and zirconium are present, and the presence of oxygen is observed, mostly, in the areas where erbium is found. Fig. 12.e)

shows the results obtained, by EDS area scanning, of the component elements in the sample $Zr_{0.25}Er_{0.75}$.

Table 5 shows the results of the quantitative analysis of the sample $Zr_{0.25}Er_{0.75}$, obtained from EDS analyses.

Table 5. Results of the quantitative analysis of sample $Zr_{0.25}Er_{0.75}$

Chemical elements	Composition measured by weighting wt.%	Composition measured by EDS wt.%	Wt.% Sigma
Zr	25	29.46	0.19
Er	75	66.44	0.20
O		4.10	0.12

Following the EDS analysis of the samples $Zr_{0.75}Er_{0.25}$ and $Zr_{0.25}Er_{0.75}$, the quantitative results confirmed that the concentrations of the component elements of both samples have been modified after the heat treatment due to the dehydrogenation of the samples, the compounds ZrH_2 and ErH_3 being separated into Zr, Er and H_2, the hydrogen being released under its pure form [12].

4. CONCLUSIONS

In the present work, an experimental study was carried out on obtaining Zr-Er compounds, which can be used in the storage and use of hydrogen as an energy source. Following these works, two sintered samples of Zr_xEr_{1-x}(x=0.25;0.75) were obtained, through the conventional process of powder metallurgy, using metal hydrides as precursors. Following the structural and morphological characterization of the samples, it was found that they have densities very close to their theoretical densities (the experimentally determined density represents over 90% of the theoretical density), the amount of zirconium used in a larger quantity leads to the appearance of an increased porosity in the sample. The size of the particles in the sintered compacts is considerably larger than the size of the raw particles, due to the bonds between the grains that appear during the sintering process, and from the EDS analyses, both samples underwent content changes, compared to the initial contents, due to dehydrogenation treatment (approximate 5-10wt.% for each component element) and erbium is more prone to oxidation than zirconium.

The intermetallic compounds obtained, through powder metallurgy, can be used for the storage and transportation of hydrogen, and how these materials were obtained presents an advantage because both the zirconium and the erbium used in this work were initially hydrided (to facilitate the subsequent processing of precursors of the sintered compounds), performing this step it is no longer necessary to perform the activation step of the materials intended for hydrogen storage.

According to the SEM analysis carried out, in the case of both types of sintered compounds, Zr and Er particles formed bonds, giving the materials a compact structure, so these materials could be used for several hydrogenation-dehydrogenation cycles.

These experimental studies will be developed in the future by characterizing the obtained samples, using other structural, morphological, and thermodynamic analysis methods, to determine the hydrogen storage capacity of sintered Zr_x-Er_{1-x} compounds.

REFERENCES

[1] Ciobanu, N.T., Schiopu, A.G., *The Annals of "Dunarea de Jos" University of Galati Fascicle IX. Metallurgy and Materials Science*, **46**(3), 5, 2023.
[2] Zuzek, E., Abriata, J., San-Martin, A., *Bulletin of Alloy Phase Diagrams*, **11**, 385, 1990.
[3] Ciobanu, N.T., Experimental studies on binary system Er-H. In *15th International Conference on Electronics, Computers and Artificial Intelligence*, Bucharest, 2023, https://doi.org/10.1109/ECAI58194.2023.10194023.
[4] Beddoes, J., Bibby, M.J., *Principles of metal manufacturing processes*, Elsevier, pp. 173-189, 1999.
[5] Chang, I., Zhao, Y., *Advances in Powder Metallurgy. Properties, Processing and Applications*, Woodhead Publishing Series, pp. 149-201, 2013.
[6] Enghag P., *Encyclopedia of the Elements. Technical Data. History. Processing. Applications*, Wiley-VCH Verlag, 2004.
[7] Mulford, R.N.R., Technical report - *A review of the rare-earth hydrides*, US Atomic Energy Comission, 1950, https://doi.org/10.2172/4310778.
[8] Dupin, N., Ansara, I., Servant, C., Toffolon, C., Brachet, J.C., *Journal of Nuclear Materials*, **275**, 287, 1999.
[9] Konigsberger, E., Eriksson, G., Oates, W.A., *Journal of Alloys and Compounds*, **299**, 148, 2000.
[10] Zhong, Y., Macdonald, D.D., *Journal of Nuclear Materials*, **423**, 87, 2012.
[11] Aurore, M., Caroline, T.M., Caroline, R., Joubert, J.M., *Calphad*, **41**, 50, 2013.
[12] Zuttel, A., *Materials Today*, **6**(9), 24, 2003.